DYNAMIC NETWORK PARTITION VIA BAYESIAN CONNECTIVITY BI-PARTITION CHANGE POINT MODEL

Zhichao Lian[1], Xiang Li[2*], Thomas Young[3], Yun Hao[4], Jianchuan Xing[5,1], Jinglei Lv[2], Xi Jiang[2], Dajiang Zhu[2], Tianming Liu[2**], Jing Zhang[1**]*

[1]Department of Statistics, Yale University, New Haven, CT; [2]Cortical Architecture Imaging and Discovery Lab, Department of Computer Science, University of Georgia, Athens, GA; [3]Department of Molecular, Cellular and Developmental Biology, Yale University, New Haven, CT; [4]School of Life Sciences, Fudan University, Shanghai, P.R. China; [5]School of Computer Science and Engineering, University of Electronic Science and Technology of China, Chengdu, P.R. China

*Joint first authors, **Joint corresponding authors.

ABSTRACT

Dynamic functional interaction has received much attention recently in the field of neuroimaging. Past studies reveal that the dynamics of functional interactions only exists in part of brain. In this paper, a novel Bayesian inference model is developed to bi-partition the brain regions into dynamic/stable sub networks and to simultaneously segment the temporal sequence of dynamic network into several states based on the interaction dynamics among regions. The accuracy of the model has been verified by synthesized data. Also, the model has been applied to a working-memory task-based fMRI dataset and interesting results on both dynamic network and change points were obtained.

Index Terms— fMRI, functional network partition, change point detection

1. INTRODUCTION

In the field of neuroimaging, there have been increasingly strong interests in the dynamic functional interaction study to understand the temporal dynamics of the brain's functional mechanism and organization, both in resting state [1, 2] and during task [3], in contrast to the traditional stationary connectivity analysis which are blind to the temporal dynamics of the brain [4]. From our previous study [5] and reports from literatures, it has been revealed that functional interactions within brain regions are locally clustered into small sub-networks [3, 6] and the dynamics of such clusters are heterogeneous. Such observations could be generalized as the hypothesis that at any certain time period, the functional interactions within only a specific, yet unknown part of brain are under dynamic process, while the interactions within most of the other brain regions remain stable. Such hypothesis, on one hand, is in accordance with the traditional functional localization theory that the response of brain to external stimulus is localized and observable in specific functionally meaningful regions. On the other hand, the hypothesis is supported by the growing evidence that additional activated regions could be identified by the changing of their functional interaction during tasks, namely the connectivity-based activation detection. Further and more importantly, by bi-partitioning the brain spatial regions into dynamic/stable sub networks and segmenting the temporal sequence into several states, we could have a simple, robust and intuitive way to study the hierarchical organization structure of the brain, bridging the concept of functional localization (by analyzing the bi-partitioning) and functional integration (by analyzing the connectives within the dynamic network) together, and be able to look at the transition pattern of such organization both with and without external stimulus.

Motivated by the importance of identifying such functional dichotomy of brain networks under a functional dynamics context, we developed a novel Bayesian connectivity bi-partition change point model (BCBCPM) to spatially characterize the localized dynamic functional network from the entire brain and temporally characterize the boundaries of temporal blocks within which the spatial distribution of the dynamic network is stable over time. In addition, to overcome the dilemma that the spatial and temporal partition result are mutually dependent and needed to be estimated simultaneously, we employ a hierarchical two-level MCMC to sample the posterior probability distribution for both results and find the optimal solution.

2. METHOD

2.1. Data acquisition

In this study, the accuracy of proposed model is first verified by datasets generated by simulating method, which would be described in detail in section 3.1. Afterwards, working memory task fMRI data is used for validating and testing the practical applicability of the model. Multimodal DTI and fMRI datasets of 19 participants were acquired during a modified version of an operational span (OSPAN) task on a 3T GE Signa scanner [7]. The total scan length was 540 seconds with TR of 2 seconds (270 volumes) and the FSL-based preprocessing details could be found in [7].

We then applied the publicly available open-source tools introduced in [8] on the structural connectome defined by each DTI dataset to obtain the 358 DICCCOL ROIs (Regions of Interest) of each individual brain and extracted the fMRI signals from those ROIs. It should be noted that the DICCCOL ROIs have intrinsic correspondences across individuals [8], thus enabling us to compare results across different subjects. Thus for each subject, the fMRI dataset is a 270*358 time series matrix and the 358 columns are in correspondence across different subjects.

2.2. Bayesian connectivity bi-partition change point model

Given the fMRI dataset obtained above, we aims to partition the DICCCOL ROIs within the whole brain of single subject into two parts: one dynamic sub network N1 that contains ROIs with temporal connectivity changes, and one stable sub network N0 that consists of the remaining ROIs without any change points. A sample case of the partitioning problem is illustrated in Fig. 1. To achieve this goal, we developed a spatial/temporal co-partitioning method separating the dynamic sub network from the entire brain, while at the same time temporally segmenting the time series to obtain the change points of the dynamic sub network.

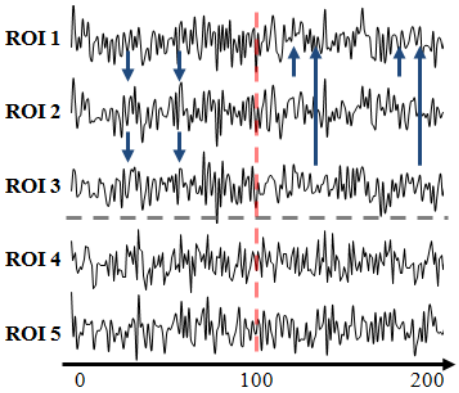

Figure 1. fMRI signals of five ROIs with one temporal change point at time point 101. The dynamic network N1 in this case consisted of 3 ROIs 1-3. In the first block, the functional interactions within the network is ROI1→ROI2→ROI3, while in the second block, the interaction pattern changes to ROI2→ROI1←ROI3; ROI4 and ROI5 are belonging to the stable sub network N0, where the functional interaction of those two ROIs are consistent over time.

Specifically, for spatial partitioning, we define a group indicator vector $S=[S_1,\ldots,S_m]$ where $S_i=1$ if the i-th ROI belongs to the dynamic sub network N1; $S_i=0$ if it is out of N1 and belonging to the stable sub network N0. For temporal partitioning, in sub network N0 we defined only one single temporal block characterizing the variation of functional interaction of the ROIs within N0. While in network N1, the time serials data will be segmented into multiple quasi-stable blocks by the indicator vector $I=[I_1,\ldots,I_n]$. $I_i=1$ if the functional interactions between the ROIs within N1 have an substantial change at the i-th time point, and I_i is defined as the starting point of a temporal block; $I_i=0$ otherwise. Thus there are totally ΣI_i blocks, as the starting time point I_1 is always considered as a change point. Finally, given group indicator vector S and block indicator vector I, the marginal likelihood of the whole fMRI data matrix $\mathbf{X}=(X_1,\ldots,X_n)$ can be written as follows:

$$p(\mathbf{X}\,|\,S,I)=p(\mathbf{X}_{N1}\,|\,S,I)p(\mathbf{X}_{N0}\,|\,S) \quad (1)$$

where $\mathbf{X}_{N1}$ denotes the time series data of all the ROIs within sub network N1 and $\mathbf{X}_{N0}$ denotes the data of all the ROIs belongs to N0, assuming the conditional independence between N1 and N0. The likelihood $p(\mathbf{X}_{N0}|S)$ in Eq. 1 can be estimated by Eq. 2 below:

$$p(X)=\frac{p(X\,|\,\mu,\Sigma)p(\mu,\Sigma)}{p(\mu,\Sigma\,|\,X)}=(\frac{1}{2\pi})^{mn/2}\left(\frac{\kappa_0}{\kappa_n}\right)^{m/2}\frac{\Gamma_m\left(\frac{\nu_n}{2}\right)}{\Gamma_m\left(\frac{\nu_0}{2}\right)}\frac{(\det(\Lambda_0))^{\nu_0/2}}{(\det(\Lambda_n))^{\nu_n/2}}2^{mn/2} \quad (2)$$

$$\Gamma_m(z)=\pi^{m(m-1)/4}\prod_{j=1}^{m}\Gamma(z+(1-j)/2)$$

where X is a set of n vectors $X_1,\ldots,X_n$ independent and identically distributed from m-dimensional multivariate normal distribution with mean of μ and covariance $\sum$. The conjugate prior distribution of (μ, $\sum$) (in numerator of Eq.2) is $N-Inv-Wishart(\mu_0,\Lambda_0/\kappa_0,\nu_0,\Lambda_0)$ [9]. The posterior distribution of (μ, $\sum$) (in denominator of Eq.2) is the similar $N-Inv-Wishart(\mu_n,\Lambda_n/\kappa_n,\nu_n,\Lambda_n)$ based on X. The details of the calculation could be referred in our previous work in [10]. The likelihood $p(\mathbf{X}_{N1}|S,I)$ can be calculated by Eq. 3 for a given block indicator vector I:

$$p(\mathbf{X}\,|\,\vec{I})=\prod_{b=1}^{\Sigma I_i}p(\mathbf{X_b}) \quad (3)$$

where $\mathbf{X_b}$ are the temporal observations belonging to bth block and $p(\mathbf{X_b})$ could be calculated according to Eq. 2.

Finally, using independent uniform priors for $p(S)$ and $p(I)$, the posterior distribution of the configuration, which is what we are interested in, could be estimated:

$$p(S,I\,|\,\mathbf{X})\propto p(S,I)p(\mathbf{X}\,|\,S,I)=p(S)p(I)p(\mathbf{X}\,|\,S,I) \quad (4)$$

2.3. MCMC scheme

Afterwards, we applied a hierarchical two-level Metropolis–Hastings scheme [11] to sample from the posterior distribution of different spatial/temporal partitioning configurations, as illustrated in Fig. 2. The lower level MCMC samples from the posterior distribution of block boundaries within the dynamic network N1 given group indicator vector S, while the higher level MCMC samples from the posterior distribution of the network structures S, i.e. the posterior probability of each node to be within N1. The proposed scheme is summarized as follows:

1. Given a random initial group indicator S^0 and random initial block indicator vector I^0, the posterior probability of the initial configuration could be obtained by Eq.4.
2. After the initialization, we will run through a low-level MCMC to sample the block boundaries within N1 by iteratively switching the values in vector I from 0 to 1 or 1 to 0 by random, thus generating a new I^*. Calculate the posterior probability of I* by Eq. 4 and set:

$$I^n = \begin{cases} I^*, & \text{if } u \le \min\left[1, \dfrac{p(S^0, I^* \mid \mathbf{X})}{p(S^0, I^{n-1} \mid \mathbf{X})}\right] \\ I^{n-1}, & \text{otherwise} \end{cases} \quad (5)$$

where u is a random number from uniform (0,1). The iteration continues until the maximum step number has been reached. In our case, the number is set as 2000 to make sure that the final posterior probability of configuration S^0/I^n converges. Record the final result as $p(S^0,I|\mathbf{X})$ i.e. the probability of S^0.
3. Propose a new group indicator vector S^* by iteratively switching the values in S by random. Given S^*, we will run a low-level MCMC as described in step 2 to find the final probability of S^* $p(S^*,I|\mathbf{X})$, then set:

$$S^n = \begin{cases} S^*, & \text{if } u \le \min\left[1, \dfrac{p(S^*, I \mid \mathbf{X})}{p(S^{n-1}, I \mid \mathbf{X})}\right] \\ S^{n-1}, & \text{otherwise} \end{cases} \quad (6)$$

where u is still a random number from uniform (0,1). Similarly, we will iterate the high-level MCMC 10000 times to make sure that $p(S^n,I|\mathbf{X})$ converges.
4. Finally, the burn-in is excluded from the actual MCMC sample of the posterior distribution and then the posterior probability for the spatial/temporal partitioning is calculated from MCMC samples.

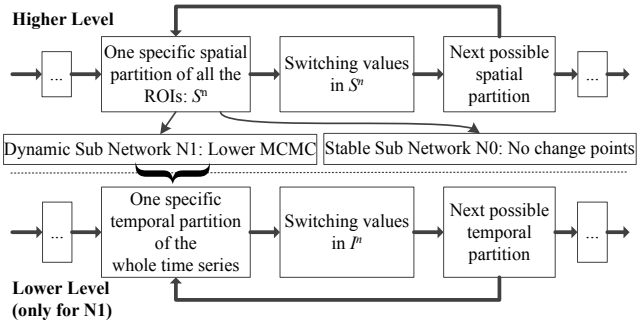

Figure 2. Diagram of two-level MCMC scheme.

3. RESULTS

3.1. Simulation results

In this study, we generated the simulation data according to the method presented in [12], which is based on the dynamic causal modeling fMRI forward model. Two sets of signals corresponding to two network types, both with 10 ROIs and time length of 400 were generated, as shown in Fig. 3a and 3b. In the first simulation, five ROIs (Y1-Y5) among all of the ten ROIs form a dynamic sub-network with a connectivity change point at time point 201. The structure of dynamic network changes from a star-like graph in the first block to an empty graph in the second block, illustrated in Fig. 3a. Each of the other five ROIs (Y6-Y10) is within the stable network independent with all of other ROIs. In the second simulation, the structure of the dynamic network changes from a ring-like graph to an empty graph at time point 201, illustrated in Fig. 3b. After running our method on the two simulation datasets, the first 5 nodes were successfully identified as within the dynamic network N1 while nodes 6-10 were grouped to N0 for both cases. The posterior probabilities for each time point being a change point within the dynamic network are depicted in Fig. 3c and 3d, showing that the change points in both simulations were accurately identified. We repeated the simulation 50 times; the error rate of the spatial/temporal partitioning results is summarized in Table 1. The low overall averaged error rates for both simulations verify the accuracy of the model.

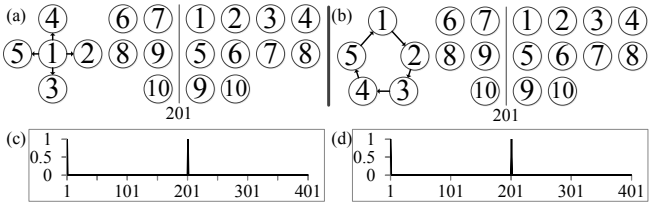

Figure 3. (a, b): Two networks generated according to the simulation method. (c, d): Temporal partitioning results, showing the posterior probability for each time point being a change point.

Table 1. Summary of Type I and Type II error rates from the model results on simulation datasets from 50 repeats.

	Type I (Spatial)	Type II (Spatial)	Type I (Temporal)	Type II (Temporal)
Simulation 1	0	0	0	0
Simulation 2	0	0	9.26%	2%

3.2. Results on real fMRI dataset

In this section, we applied the proposed BCBCPM to the fMRI dataset described in 2.1. Across the 19 subjects, the average number of ROIs within the dynamic network N1 is 319.58 and the standard variance is 6.61. More interestingly, there are 85 common ROIs involved in the dynamic networks of all subjects as visualized in Figure 4b. Based on these observations, we hypothesize that these 85 ROIs are the "engine of functional brain dynamics" during the working-memory task, as they are consistently involved in dynamic network, playing the central role of the functional interaction dynamics and transitions.

In addition, the detected change points within the dynamic network N1 are shown in Figure 4a. There are 14 change points detected for 17 subjects except subject #4 (12 change points) and #12 (13 change points). As each of the 17 subjects has a sequence of change points detected and the length of the sequence is the same, we obtained the mean position and its variance of each change point across 17 subjects, and the values are shown in Table 2. We also listed

the starting positions of each stimulus defined in the task design paradigm in Table 2. The result shows that the sequence of change points detected by the proposed method are well in correspondence with the boundaries between task and baseline, with very small variance across subjects. As various studies have shown that the activation pattern of different localized regions in the brain are responding to the external stimulus, the correspondence between the change points and the stimulus boundaries validates our method in the sense that the change points detected are reliable and neuroscientifically meaningful.

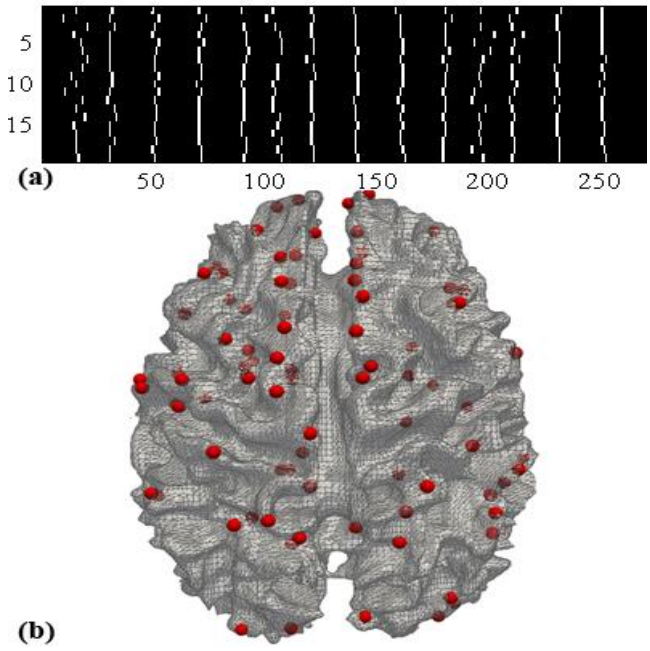

Fig. 4 (a) Change points detected in N1 for all 19 subjects, the x-axis is the temporal indices, the y-axis is the subject indices, cells highlighted by white are change points. (b) Visualization of the 85 common ROIs as red spheres on cortical surface of all 19 subjects.

Table 2 The mean position and variance for each change point

Change Point	Mean Position	Standard Deviation	Task Boundary
#1	16.71	2.44	NA
#2	31.65	1.06	31
#3	51.41	1.00	51
#4	71.41	0.71	71
#5	91.12	0.86	91
#6	105.88	1.58	NA
#7	121.47	0.62	121
#8	141.24	0.66	141
#9	161.41	0.94	161
#10	180.88	0.78	181
#11	196.76	2.61	NA
#12	211.76	1.35	211
#13	231.47	0.80	231
#14	251.35	0.70	251

Furthermore, we detected 3 unexpected yet functional meaningful change points (#1, #6, and #11) which are not explicitly corresponding to the boundaries between task and baseline. All these three change points are located in the time period during task 1, which has two stages: in the first 40 seconds participants were required to memorize a character, and after that they were asked to answer a question regarding the character. Therefore, these three change points are probably caused by the different stages in task 1 and the results show the potential of our model in detecting the extra change points of brain functional interaction in addition to the task design information.

4. DISCUSSION AND CONCLUSION

In this study, we have presented a novel Bayesian inference model for spatially localizing a dynamic network from the entire brain and temporally detecting the boundaries of temporal blocks which exhibit substantial differences of functional connectivity within the dynamic network. The concept of localized dynamic network could provide a new scope for analyzing brain functional interaction and its dynamics. In this work, we applied the proposed method on task-based fMRI dataset and obtained meaningful results which could be further investigated to reveal the hidden functional interaction dynamics during task. Also, as illustrated in 3.2, our method could do the temporal/spatial partition without any a priori information, thus it also could be to be applied on resting-state fMRI data in the future.

5. REFERENCES

[1] W. Majeed, *et al.*, "Spatiotemporal dynamics of low frequency BOLD fluctuations in rats and humans," *NeuroImage,* vol. 54, no. 2, pp. 1140-1150, 2011.

[2] C. Chang, and G. H. Glover, "Time-frequency dynamics of resting-state brain connectivity measured with fMRI," *NeuroImage,* vol. 50, no. 1, pp. 81-98, 2010.

[3] X. Zhang, *et al.*, "Characterization of task-free and task-performance brain states via functional connectome patterns," *Medical Image Analysis,* vol. 17, no. 8, pp. 1106-1122, 2013.

[4] N. Leonardi, *et al.*, "Principal components of functional connectivity: A new approach to study dynamic brain connectivity during rest," *NeuroImage*, in press, 2013.

[5] X. Li, *et al.*, "Dynamic functional connectomics signatures for characterization and differentiation of PTSD patients," *Human Brain Mapping*, pp. in press, 2013.

[6] D. S. Bassett, and E. Bullmore, "Small-World Brain Networks," *The Neuroscientist,* 12, 512-523, 2006.

[7] C. C. Faraco, *et al.*, "Complex span tasks and hippocampal recruitment during working memory," *NeuroImage,* 55, 2011.

[8] D. Zhu, *et al.*, "DICCCOL: Dense Individualized and Common Connectivity-Based Cortical Landmarks," *Cerebral Cortex*, April 5, 2012.

[9] A. Gelman, *et al.*, "Bayesian Data Analysis," 2003.

[10] J. Zhang, *et al.*, "Inferring Functional Interaction and Transition Patterns via Dynamic Bayesian Variable Partition Models," *Human Brain Mapping*, in Press.

[11] J. S. Liu, "Monte Carlo Strategies in Scientific Computing," Springer, 2001.

[12] S. M. Smith, *et al.*, "Network modelling methods for FMRI," *NeuroImage,* 54, 875-891, 2011.